Journal of Materials Science: Materials in Electronics (2020) 31:4672–4676
https://doi.org/10.1007/s10854-020-03019-0

Growth of $PbBr_2$ microrods with unique structure and surface morphology

Zubair Ahmad[1] · **Arti Mishra**[1]

Received: 11 January 2020 / Accepted: 29 January 2020 / Published online: 8 February 2020

Abstract
We describe an innovative method to fabricate the one-dimensional (1D) microrods of lead bromide ($PbBr_2$). The microrods possess unique structural and morphological properties. XRD, FESEM and HRTEM analysis exhibited a well-ordered growth and a crack-free arrangement of the microcrystals in rod shapes. XPS, Raman and FTIR studies were performed to investigate the composition and chemical structure of the rods. TGA and DSC investigations were made to investigate the thermal stability of microrods. The growth of these unique 1D microrods represents an innovative concept in material design and synthesis, which can foster a revolutionary research in the field of perovskite crystals.

1 Introduction

During the last few years, a large number of studies have been performed to develop the lead halide crystals due to their interesting optoelectronic properties [1]. Interestingly, lead halides can make multidimensional crystal networks using a similar unit structure [2]. Typically, in the case of bulk crystals, the dimensions of the lead halide crystals are in the range of centimetres and offers limited flexibility for practical applications [3]. On the other hand, in the case of nanosized crystals, it is difficult to achieve good optoelectronic properties and decent atomic consistency. Also, the conventional crystal growth procedure requires a seed and a specific environment [4, 5]. Therefore, the development of simple and more economical methods for the crystal growths is vital [6].

As compared to the film analogues, crystalline structures offer more fascinating optoelectronic properties [7]. These distinctive properties result from their considerable surface-to-volume ratio, strong light absorption and facile fabrication methods [8]. A consistent regular distribution and alignment of the crystalline structures are more appropriate for the perovskite-based photodetectors applications and beyond.

In the present study, we synthesized the 1D microrods of $PbBr_2$ using solution-based facial growth technique. The morphological, structural, thermal and chemical properties of the microrods have been studied using various characterization tools. To the best of our knowledge, this is the first report of $PbBr_2$-based 1D microcrystalline rods consisting of such interesting structural and morphological characteristics.

2 Experimental

Lead (II) Bromide ($PbBr_2$) power was purchased from Lumtec (Taiwan), while the di-methyl-formamide (DMF) (anhydrous, 99.8%) was obtained from Agros chemicals. To synthesize the 1D microrods, 1 M solution of $PbBr_2$ in dimethylformamide (DMF) was prepared by heating the DMF at 100 °C in a sealed container. Then the solution was kept in a stable place for two weeks. After 10 days, the crystals were started visualizing in the solution and they took a few more days to grow longer. Detail characterization and the schematic of the procedure are given in supplementary data file (see Fig. S1). Figure S2 shows the photos of the $PbBr_2$ and $CH_3NH_3PbBr_3$ solution during the crystal growth. Here it is important to mention that initially both the solutions were transparent; however, in the case of $PbBr_2$ the solution turned to coloured once the crystalline growth was started. JEOL 7600 SEM was used to study the surface

Electronic supplementary material The online version of this article (https://doi.org/10.1007/s10854-020-03019-0) contains supplementary material, which is available to authorized users.

✉ Zubair Ahmad
zubairtarar@qu.edu.qa

[1] Center for Advanced Materials (CAM), Qatar University, P. O. Box 2713, Doha, Qatar

morphology. TGA and DSC studies were performed using the Perkin Elmer TGA 4000 Analyzer and Perkin Elmer DSC 8500 system, respectively. Jobin-Yvon HR800 Raman spectrometer was used to record the Raman Spectra. FTIR spectra were obtained using Spectrum 2000, USA (Perkin Elmer). XRD patterns were measured by using the EMPYREAN X-ray-diffractometer. Compositional analysis was performed using AXIS Ultra DLD XPS system.

3 Results and discussion

X-ray diffraction (XRD) spectra of the $PbBr_2$ crystalline rods (cyan circles) and crystalline powder (black lines) are shown in Fig. 1a. Both spectra exhibit an orthorhombic system (P n m a (624) space group) with $a = b = 0.8059$ nm and $c = 0.4732$ of $PbBr_2$ (hematite, JCPDS file No. 07-0235). However, the $PbBr_2$ microcrystalline rods have a very well-oriented development in the direction along the a-axis. In the case of the crystalline rods, the exciton absorption bands shifted towards the shorter wavelength (blue shift). In the case of $PbBr_2$ crystalline rods, the intensity of the peaks is much higher as compared to the $PbBr_2$ powder. The prominent peaks have been detected at 14.37°, 18.58°, 21.63°, 22.04° and 23.69° corresponding to the (101), (002), (011), (102) and (111) lattice planes of the $PbBr_2$. (112) and (211) lattice planes have been found at the diffraction angles of 28.76° and 30.58°, respectively. It can be noticed that the d-spacing of the $PbBr_2$ crystalline rods is higher as compared to $PbBr_2$ powder ensuing the shift of the lattice planes towards the lower diffraction angles. The shifting of the d-value may be due to the reordering of lattice positions during the growth of the rods [9]. The high-intensity XRD peaks attained at 9.5° and 12.3° represent the highly crystalline nature of the preparation phase. The existence of anonymous peaks proposes a new in-between phase, which may be due to the complex of the $PbBr_2$-DMF [10]. The EDS results are given in Fig. S3(a). The peaks at 2.48 and 10.5 keV denote the lead while the other two peaks (at 1.5 and 11.75 keV) can be assigned to Bromine. In the $PbBr_2$

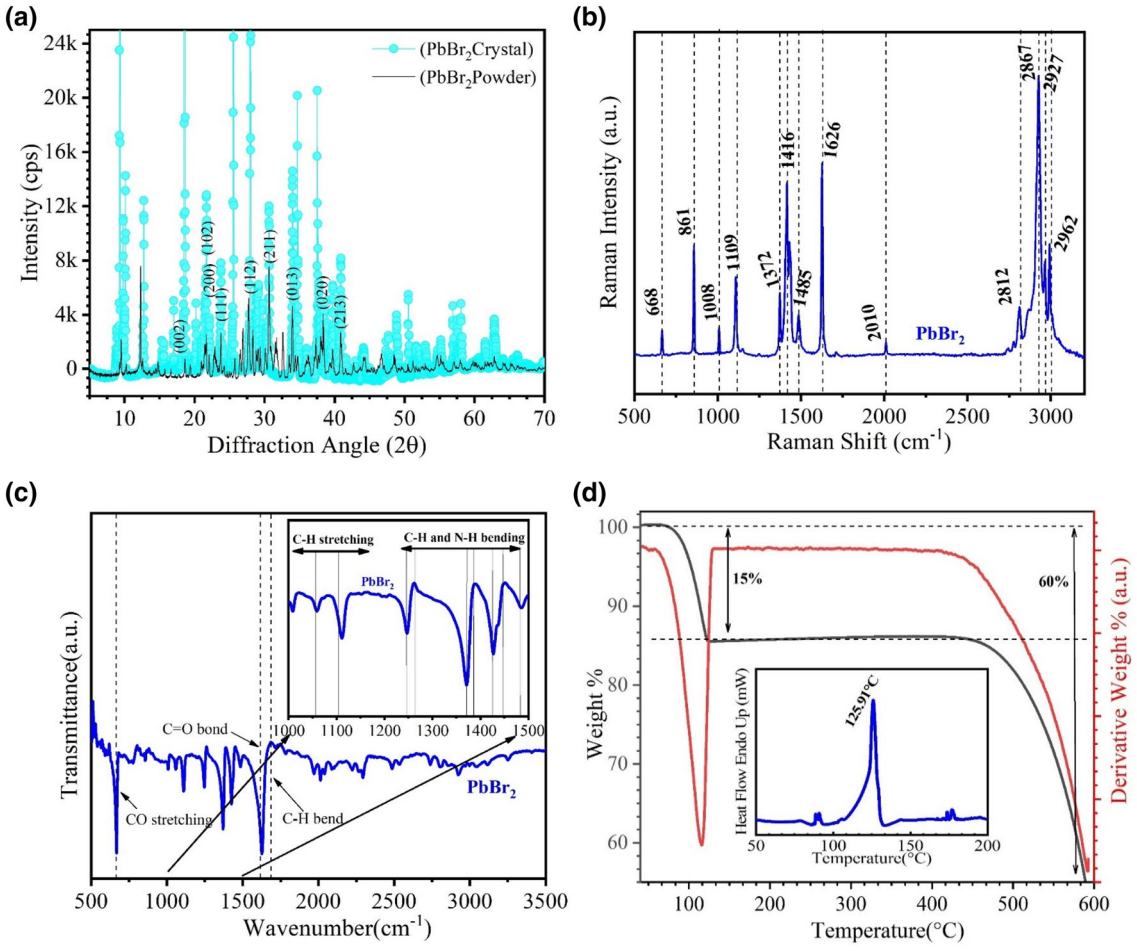

Fig. 1 a Diffraction patterns of $PbBr_2$ powder and $PbBr_2$ microcrystalline rods. b Raman spectra of $PbBr_2$ microrods. c FTIR spectra of $PbBr_2$ microrods. d TGA weight loss curves and the DSC heating curve (inset) $PbBr_2$ microcrystalline rods

microcrystalline rods, the atomic composition of Pb and Br was found to be 1:2.28, which refers to the development of pure phases.

Raman spectrum (Fig. 1b) exhibits the internal vibration due to the C–N stretching, CH_3 and NH_3 bending, and CH_3 and NH_3 stretching around 600–1100 cm^{-1}, 1300–1600 cm^{-1} and 3000 cm^{-1}, respectively. The FTIR results are shown in Fig. 1c demonstrating the existence of the vibrations at 860 cm^{-1} and 660 cm^{-1} corresponding to the C–N and C–O stretching. The climaxes at 1007 cm^{-1} and 1058 cm^{-1} belong to sp^3 (C–H) stretching. The peaks in the range of 1250–1550 cm^{-1} matched with the C–H and N–H bending. Stretching vibration because of the C=O bond appeared at 1620 cm^{-1} and 1660 cm^{-1}. The FTIR features (in the range of 500–1700 cm^{-1}) are well matched to the Raman spectrum. Nevertheless, some peaks presented in the Raman spectra are absent in the FTIR spectra over the 1700 cm^{-1}. This is owing to the fact that in the Raman measurements the vibrational energies are activated because of the changes in polarization while the FTIR active intensities are dependent on the dipole moment [11]. The description of the thermal characteristics (Fig. 1d) is given in the supplementary data. The Raman, FTIR (Fig. 2) and XPS (Fig. 3) results indicate the presence of CH– and NH– groups, which should not be observed in $PbBr_2$. The existence of CH– and NH– groups is maybe due to the solvent (DMF in this case). We had performed the experiments to develop the microrods of the both $PbBr_2$ and $CH_3NH_3PbBr_3$. In the case of $CH_3NH_3PbBr_3$ perovskite solution in DFM, no growth of the rods has been found (see the attached photo in the supplementary data, Fig. S2).

TGA was used to find the thermal stability (see Fig. 1d). The weight loss is detected in two temperature ranges. The first weight loss was found at ~ 115 °C due to the evaporation of moisture in the materials [12]. The second weight loss was detected at ~ 580 °C and the sequential decomposition has been found in the material [13]. Our TGA results are in a good agreement with the previously reported data [12, 14]. DSC results (in the inset of Fig. 1d) show a sharp endothermic peak at 126 °C which can be attributed to the polymorphic transformation during the heating procedure [15].

Figure 2 illustrates the structure and morphology of the crystalline rods using the FESEM images. The crystals grow in longitudinal dimension having the lengths up to 5 mm, while the diameter of the rods is in the range of 10–100 µm. The FESEM images also show that the $PbBr_2$ crystalline rods are consisting of porous structure with submicron size pores. The magnified FESEM images of the rods illustrate that several micro-structures are linked in the longitudinal direction to form the microcrystalline rods. As a result of the

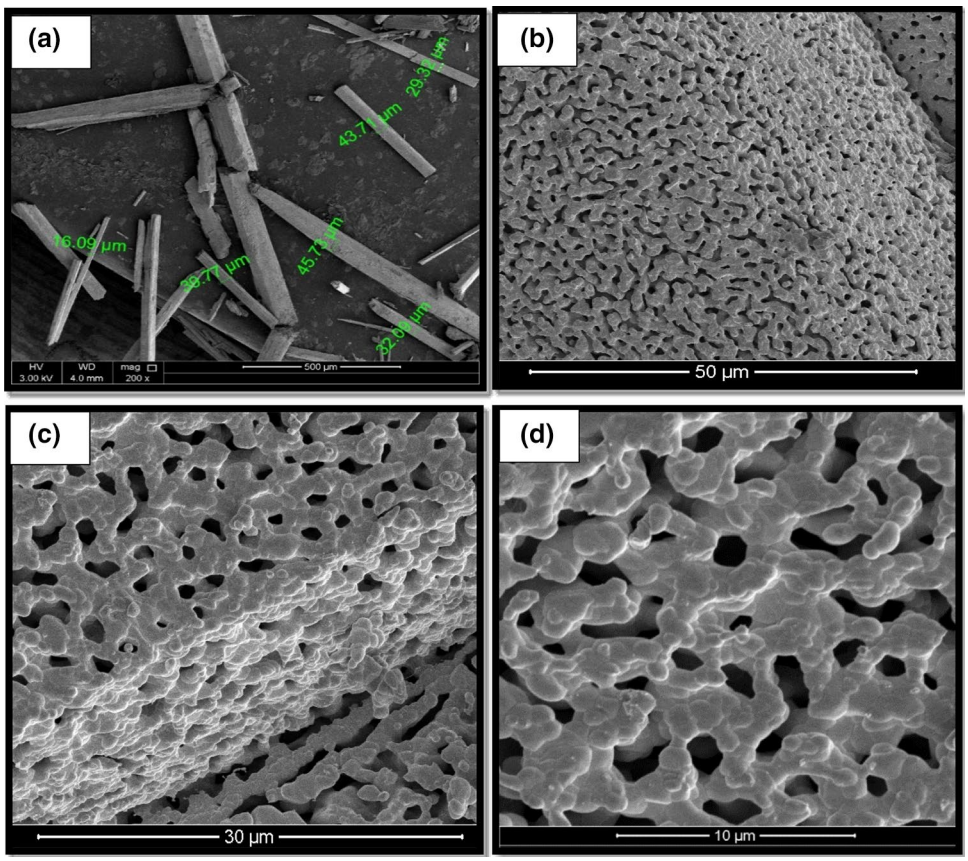

Fig. 2 FESEM images of the $PbBr_2$ 1D microcrystalline rods, captured at different magnifications

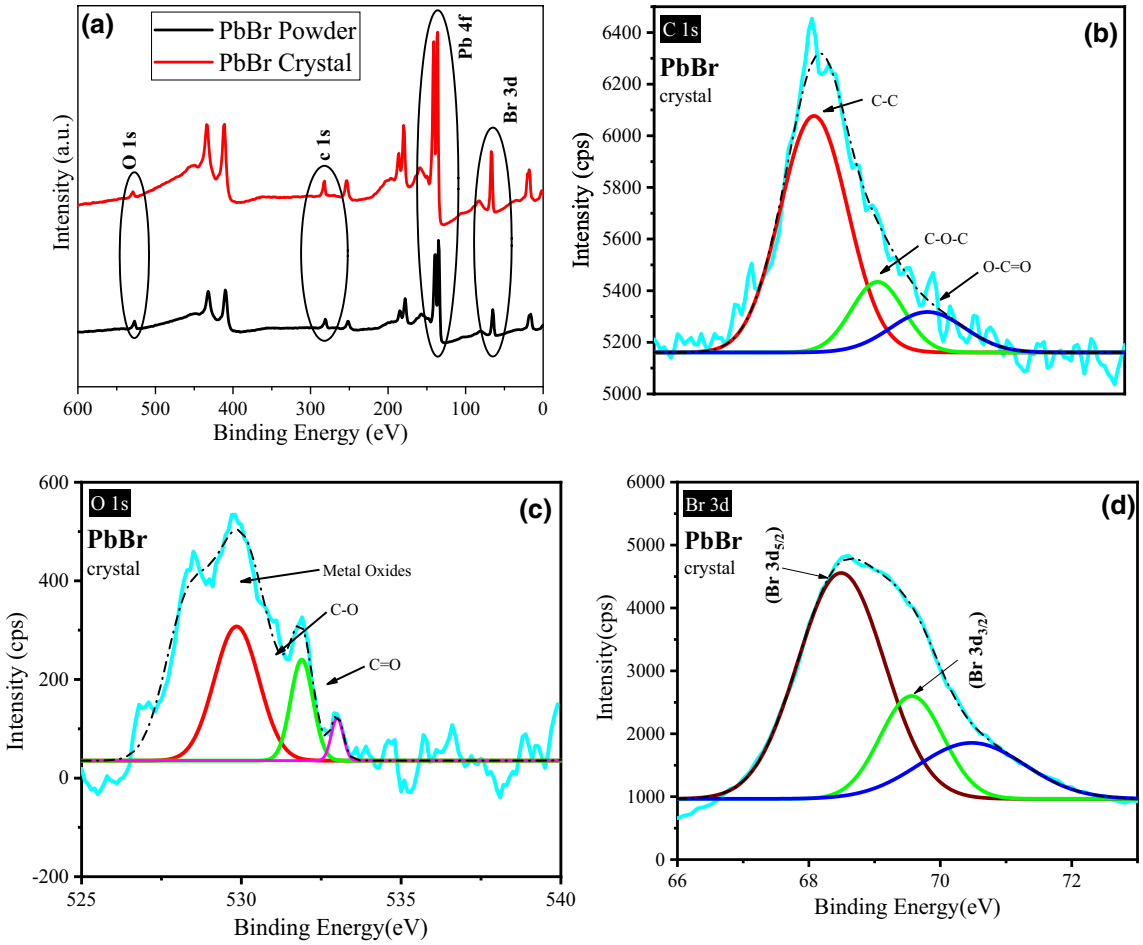

Fig. 3 **a** XPS survey spectra of the $PbBr_2$ 1D crystalline rods and $PbBr_2$ powder. **b–d** The core-level XPS spectra of carbon (C 1s), oxygen (O 1s) and bromide (Br 3d)

minor variation in the dimensions of the micro-structures, a small gap between the head-to-head micro-structures results in the creation of micro-pores. Nevertheless, no head-to-head cracks or any visual defect has been found on the surface of the microcrystalline rods. The HRTEM images [Fig. S3(b), supplementary data] were taken at the certain area to investigate the presence of any pores on the surface of the connected micro-structures in the microrods. However, there is no proof of any crack or nano-pores on the surface of the connected micro-structures in the microrods. More high-resolution TEM micrographs of $PbBr_2$ crystalline rods cannot be taken since the $PbBr_2$ crystals have been found to be very sensitive to high-energy electron beam, which may cause distortion in the crystal structure.

To determine the elemental composition, XPS spectra of the rods were recorded in the range of 0 to 800 eV. The elemental composition of the rods contains lead, bromide, carbon and oxygen. In C1s spectra (Fig. 3b), the intensity of carbon peaks expressively improves after crystal growth and the peaks at 284.6, 286.3 and 288.3 EV are referred to C–C, C–O–C and O–C=O bonds, respectively [16]. The peak positions are consistent with powder samples as well. In the O1s (Fig. 3c) spectra, the peaks at 529, 531.5, and 533 eV can be assigned to the metal oxides, C–O bond and C=O bond, respectively. Figure 3d shows the two distinguished peaks of Bromine at 68.5 eV and 70.1 eV correspond to the Br $3d_{5/2}$ and Br $3d_{3/2}$. The intensity of bromine peaks has significantly improved in the crystals as compared to lead bromide powder. The core-level spectrum of lead (Fig. S3) shows two different peaks, the 1st at 136.8 eV envisioned for Pb $4f_{7/2}$ and the 2nd at 141.6 eV anticipated for Pb $4f_{5/2}$ [17]. Pb 4f region has well-separated spin-orbit components with $\Delta = 4.87$ eV (see Fig. S4, supplementary data).

4 Conclusion

The XRD spectrum of the microcrystalline rods displays the orthorhombic system (P n m a (624) space group). FTIR spectrum reveals the presence of a strong interaction

among the N–H and C–H groups in the 1D crystalline rods which have also been confirmed by Raman spectroscopy which might be due to the impurities originated from the solvent (DMF). FESEM and HRTEM confirm the microporous structure of the 1D crystalline rods with head-to-head crack-free morphology. TGA and DSC studies show that the thermal behaviour of 1D microcrystalline rods is in a good agreement with the previous reports. The development of these unique 1D microrods suggests a new concept in perovskite crystal synthesis for the application in the optoelectronics and beyond.

Acknowledgements Open Access funding provided by the Qatar National Library. This work was supported by Qatar University Internal Grant Nos. QUCG-CAM-2018/19-1 and NPRP11S-1210-170080 from Qatar National Research Fund (a member of Qatar Foundation). The findings achieved herein are solely the responsibility of the authors.

Compliance with ethical standards

Conflict of interest The authors declare that there is no conflict of interest.

References

1. D. Głowienka, J. Szmytkowski, Numerical modeling of exciton impact in two crystalographic phases of the organo-lead halide perovskite ($CH_3NH_3PbI_3$) solar cell. Semicond. Sci. Technol. **34**, p. 035018, (2019).
2. T. Qiu, Y. Hu, F. Xu, Z. Yan, F. Bai, G. Jia, S. Zhang, Recent advances in one-dimensional halide perovskites for optoelectronic applications. Nanoscale **10**, 20963–20989 (2018)
3. Z. Liu, B. Sun, X. Liu, J. Han, H. Ye, T. Shi, Z. Tang, G. Liao, Efficient carbon-based $CsPbBr_3$ inorganic perovskite solar cells by using Cu-phthalocyanine as hole transport material. Nano Micro Lett. **10**, p. 34, (2018).
4. D. Bi, W. Tress, M.I. Dar, P. Gao, J. Luo, C. Renevier, K. Schenk, A. Abate, F. Giordano, J.P. Correa Baena, J.D. Decoppet, S.M. Zakeeruddin, M.K. Nazeeruddin, M. Gratzel, A. Hagfeldt, Efficient luminescent solar cells based on tailored mixed-cation perovskites. Sci. Adv. **2**, e1501170 (2016)
5. J. Huang, Q. Dong, Method for single crystal growth of photovoltaic perovskite material and devices, in: U.S. Patent (ed.), NUtech Ventures, Lincoln, NE (US), 2017
6. L. Etgar, The merit of perovskite's dimensionality; can this replace the 3D halide perovskite? Energy Environ. Sci. **11**, 234–242 (2018)
7. R. Agarwal, C. Lieber, Semiconductor nanowires: optics and optoelectronics. Appl. Phys. A **85**, p. 209, (2006).
8. O. Hayden, R. Agarwal, C.M. Lieber, Nanoscale avalanche photodiodes for highly sensitive and spatially resolved photon detection. Nat. Mater. **5**, 352 (2006)
9. P. Beckmann, ChemInform abstract: a review of polytypism in lead iodide. Cryst. Res. Technol. **45**, pp. 455–460, (2010).
10. B.R. Vincent, K.N. Robertson, T.S. Cameron, O. Knop, Alkylammonium lead halides. Part 1. Isolated PbI_{64}—ions in $(CH_3NH_3)4PbI_6.2H_2O$. Can. J. Chem. **65**, pp. 1042–1046, (1987).
11. E. Mosconi, C. Quarti, T. Ivanovska, G. Ruani, F. De Angelis, Structural and electronic properties of organo-halide lead perovskites: a combined IR-spectroscopy and ab initio molecular dynamics investigation. Phys. Chem. Chem. Phys. PCCP **16**, pp. 16137–16144, (2014).
12. B.D. Fahlman, A.R. Barron, Substituent effects on the volatility of metal β-diketonates. Adv. Mater. Opt. Electron. **10**, 223–232 (2000)
13. T. Baikie, Y. Fang, J.M. Kadro, M. Schreyer, F. Wei, S.G. Mhaisalkar, M. Graetzel, T.J. White, Synthesis and crystal chemistry of the hybrid perovskite $(CH_3NH_3)PbI_3$ for solid-state sensitised solar cell applications. J. Mater. Chem. A **1**, pp. 5628–5641, (2013).
14. Y. Liu, Z. Yang, D. Cui, X. Ren, J. Sun, X. Liu, J. Zhang, Q. Wei, H. Fan, F. Yu, X. Zhang, C. Zhao, S.F. Liu, Two-inch-sizedperovskite $CH_3NH_3PbX_3$ (X = Cl, Br, I) crystals:growth and characterization. Adv.Mater. (Deerfield Beach, Fla.) **27**, pp. 5176–5183, (2015).
15. T. Supasai, N. Rujisamphan, K. Ullrich, A. Chemseddine, T. Dittrich, Formation of a passivating $CH_3NH_3PbI_3/PbI_2$ interface during moderate heating of $CH_3NH_3PbI_3$ layers. Appl. Phys. Lett. **103**, p. 183906, (2013).
16. S. Yuan, P. Zhang, Z. Yang, L. Lv, S. Tang, B. Liang, Successive grafting of poly(hydroxyethyl methacrylate) brushes and melamine onto chitosan microspheres for effective Cu(II) uptake. Int. J. Biol. Macromol. **109**, 287–302 (2018)
17. J. An, Y.B. Liu, Y. Lu, The influence of Pb on the friction and wear behavior of Al–Si–Pb alloys. Mater. Sci. Eng. A **373**, pp. 294–302, (2004).